Soft Matter

Dynamic Article Links

Cite this: *Soft Matter*, 2012, **8**, 3810

www.rsc.org/softmatter

PAPER

Electrodeformation method for measuring the capacitance of bilayer membranes

Paul F. Salipante,[ab] Roland L. Knorr,[b] Rumiana Dimova[b] and Petia M. Vlahovska*[a]

Received 4th November 2011, Accepted 23rd January 2012
DOI: 10.1039/c2sm07105c

We report a novel non-invasive method to measure the capacitance of biomimetic bilayer membranes. The approach utilizes the frequency-dependent deformation of giant unilamellar vesicles in AC uniform electric field. The method is applied to membranes made of lipids and polymers. Compared to lipid membranes, polymer bilayers have an order of magnitude lower capacitance, which correlates with their larger thickness. The capacitance of both lipid and polymer bilayers is found to be voltage-independent in the examined range between 2 and 6 kV m^{-1}, indicating membranes do not experience significant thinning due to electrostriction.

1 Introduction

Electric properties of biomembranes play a pivotal role in cellular functions,[1] *e.g.*, synaptic efficacy and electric signal propagation in neurons,[2–4] as well as biomedical applications,[5] *e.g.*, gene transfection, where the controlled application of electric pulses induces transient pores in the cell membrane thereby enabling the delivery of foreign DNA into the cell.

The main structural component of biological membranes is the lipid bilayer, which is impermeable to ions. Upon application of an external electric field, charges accumulate on the two sides of the membrane setting up a potential difference, *i.e.*, the membrane acts as a capacitor. The capacitive nature of the plasma membrane is crucial for cell viability in external electric fields because it helps shield the cell interior. If the capacitor is fully charged, it draws zero current and the voltage drop occurs entirely across the membrane; the external electric field does not penetrate the cell. However, the charging of the membrane capacitor occurs over a period of time (on the order of few microseconds at physiological conditions) during which the cell interior participates in the conduction process. Thus, nanosecond electric pulses affect the intracellular content and have been used, for example, for nucleus electroporation.[6,7] The transient capacitive charging can also destabilize and disrupt the plasma membrane,[8] resulting in the irreversible loss of the barrier function and cell death.

The charging time scale depends on the membrane capacitance,[9] hence accurate knowledge of this parameter is needed in order to better control cell interactions with electric fields. Existing methods to measure plasma membrane capacitance of real cells include classic electrophysiological techniques such as patch-clamp,[10] electromechanical methods based on individual cell dielectrophoresis, electrorotation and electro-orientation,[11] and dielectric spectroscopy based on the frequency-dependent permittivity and conductivity of suspensions of cells[12–14] or liposomes.[15] The patch-clamp method is very effective, but can be invasive and laborious. Dielectric spectroscopy is non-invasive and can be applied to measure membrane potential of live cells,[16] and structural organization of the lipid bilayer.[15] However, this technique requires complex equipment and monodisperse suspensions; probing the collective response of polydisperse suspension of cells (or vesicles) yields only an average value of the membrane electric properties. The low-throughput and difficulties associated with the existing methods motivated our effort to establish a new and facile method for measuring the membrane capacitance of lipid bilayers.

A model membrane system provides a better defined experiment and the means of interrogating membranes of various composition of interest in isolation. A classic example is the artificial lipid bilayer (BLM).[17–19] Voltage- or current- clamp methods for measuring the capacitance of BLMs,[20–24] recently reviewed in ref. 25, have yielded a wealth of data. However these techniques are limited by BLM fragility. BLMs usually retain some of the solvent used for their formation; thus, they are thicker than the bilayer portion of a biological membrane. In the past 15 years, another system has gained popularity as a model to study membrane biophysics: giant unilamelar vesicles, which are cell-size membrane envelopes.[26] Their large size (10–100 μm) allows for direct observation of the dynamic response of individual vesicles to electric fields using real time optical microscopy.[27,28] Yet another advantage of giant vesicles compared to BLMs is the possibility for tension control in the system. High tensions characteristic for BLMs could result in bilayer thinning.

Vesicles aspirated in a micropipette have been employed to study the electromechanical properties and limits of lipid and

[a]*School of Engineering, Brown University, Providence RI 02912, USA. E-mail: petia_vlahovska@brown.edu; Fax: +1 401 8639028; Tel: +1 401 8639774*
[b]*Department of Theory and BioSystems, Max Planck Institute of Colloids and Interfaces, Science Park Golm, 14424 Potsdam, Germany*

polymer membranes.[29,30] Freely suspended quasi-spherical vesicles (vesicles whose equilibrium shape is a sphere but excess area is stored in submicron fluctuations) deform into ellipsoids when subjected to a uniform AC electric field.[31–34] If the inner fluid is less conducting than the suspending medium, as the frequency is increased the vesicle changes its shape from a prolate to oblate ellipsoid, *i.e.* at low frequencies the vesicle elongates in the field direction, while at higher frequencies the vesicle's long axis is perpendicular to the applied field. The transition frequency depends on the membrane charging time.[35–37]

In this paper, we demonstrate how the prolate–oblate transition can be exploited to infer membrane capacitance. Giant vesicles from artificial and natural lipids are relatively easy to prepare using the electroformation method. The measurement itself requires a frequency sweep which can be quickly and easily done with either home-made or commercially available electroporation chambers. Finally, the method is non-invasive as it does not require any direct contact with the membrane. We apply the method to membranes assembled from lipids and block-copolymers. The latter form shells (polymersomes) that have been subject to increasing interest as drug-delivery systems.[38,39]

2 Physical and theoretical basis of the experimental method

Typical experimental observations of the evolution of the vesicle shape with frequency in a uniform AC fields is illustrated in Fig. 1. The degree of deformation is quantified by the aspect ratio $D = a_{\parallel}/a_{\perp}$, where $a_{\parallel}$ is parallel and $a_{\perp}$ is normal to the field direction; see inset of Fig. 1. A quasi-spherical vesicle (made of neutral lipids or polymers) adopts either prolate or oblate ellipsoidal shape, depending on the ratio of the conductivities of the enclosed and suspending solutions λ_{in} and λ_{ex} respectively,

$$\Lambda = \frac{\lambda_{in}}{\lambda_{ex}}. \quad (1)$$

At low frequencies, in the sub-kHz range, the vesicle shape is always a prolate ellipsoid regardless of the solution conductivities. At high frequencies (above MHz), the vesicle remains a sphere. At intermediate frequencies, a vesicle filled with a less conducting solution, $\Lambda < 1$, deforms into an oblate ellipsoid. The change in shape occurs in the 1–100 kHz range. Around this transition frequency, the prolate deformation of a vesicle characterized by $\Lambda > 1$ increases. The physical mechanism underlying these shape variations in an AC field is illustrated in Fig. 2. In essence, depending on the relative magnitude of the period of the field reversal, *i.e.*, the field frequency, and the capacitor charging time, the bilayer capacitor is either fully-charged or short-circuited. In the latter case, since the inner fluid participates in the conduction process, the vesicle polarization becomes dependent on Λ.[35]

For a quasi-spherical vesicle of radius a, modeled as a spherical thin insulating shell of thickness h ($h \ll a$) and dielectric permittivity ε_m, the frequency at which the transition between prolate and oblate shape is theoretically predicted to occur is[36,40]

$$f_c = \frac{\lambda_{in}}{2\pi a C_m}[(1-\Lambda)(\Lambda+3)]^{-1/2}, \quad (2)$$

where $C_m = \varepsilon_m/h$ is the specific membrane capacitance. Eqn (2) is valid if the inner and outer fluids have the same dielectric constant, which is indeed the case of vesicles, where both interior and suspending fluids are aqueous solutions. Notably, the transition frequency is not exactly the inverse of the capacitor charging time, which in the case of a spherical capacitor is[41]

$$t_m = \frac{aC_m}{\lambda_{in}}\left(1+\frac{\Lambda}{2}\right). \quad (3)$$

Eqn (2) is the basis of our approach for deducing the membrane capacitance. The experiment reduces to selecting a quasi-spherical vesicle at conductivity conditions corresponding to $\Lambda < 1$, and subjecting it to a frequency sweep in the range 0.1–20 000 kHz and field strength 2–6 kV m^{-1}. The frequency at which the value of the measured aspect ratio is $D = 1$ yields f_c, which is used to deduce the membrane capacitance *via* eqn (2).

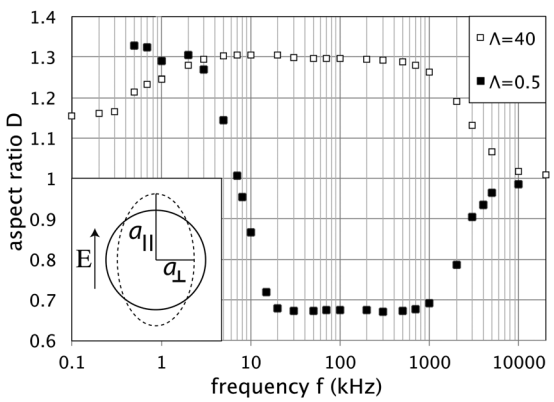

Fig. 1 Frequency dependent deformation of polymersomes with $\Lambda = 40$ (□) and $\Lambda = 0.5$ (■) exposed to a 6 kV m^{-1} AC field. For $\Lambda = 40$, an increase in elongation is observed in the 1–100 kHz range, while at these frequencies for $\Lambda = 0.5$ the vesicle changes shape from a prolate to an oblate ellipsoid. Aspect ratio $D > 1$ indicates prolate shape (vesicle elongation in the field direction), while $D < 1$ corresponds to oblate shape. In both cases, the vesicle shape becomes spherical in the MHz frequency range. Increasing or decreasing frequency sweep shows no hysteresis. Polymersome radii are 41 μm (□) and 18 μm (■).

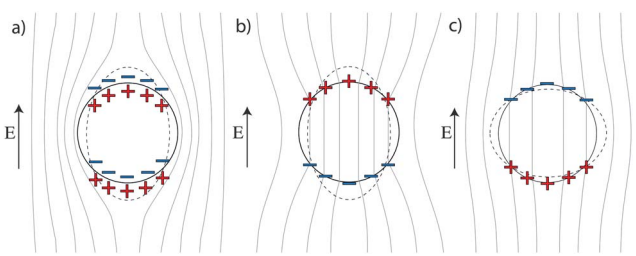

Fig. 2 The steady electric field around a vesicle immersed in an electrolyte solution, following the imposition of a background uniform AC field. (a) At low frequencies, $f < f_c$, the capacitor is fully charged. (b) and (c) At intermediate frequencies, $f > f_c$, it is short-circuited and there is charge imbalance between the inner and outer membrane surfaces. (b) If the enclosed solution is more conducting than the suspending medium, $\Lambda > 1$, the vesicle is pulled into an prolate ellipsoid. (c) The polarization is reversed in the opposite case $\Lambda < 1$ and the vesicle deforms into an oblate ellipsoid.

3 Materials and experimental procedures

3.1 Preparation of giant vesicles

Giant vesicles are prepared from the lipid palmitoylphosphatidylcholine (POPC) and s-Bu-[CH_2–$CH(C_2H_3)$]$_n$–[O–CH_2–CH_2]$_m$–OH diblock copolymers (denoted as PBd$_n$-*b*-PEO$_m$) using the electroformation method.[42] The names and properties of the polymers are listed in Table 1. The lipids were purchased from Avanti. The copolymers PS1, PS3 and PS4 were obtained from Polymer Source Inc. (Montreal, Canada), while PS2 was available in the lab,[43] originally synthesized by Förster and Krämer.[44] The polymers were chosen to have hydrophilic fraction ϕ similar to lipids in order to ensure formation of giant vesicles and not other structures, *e.g.*, micelles.[38] The dry polymer melts were stored in the freezer at −20 °C. All materials were used without further purification. Stock solutions with concentration 10 mg ml^{-1} were made using chloroform.

In the electroformation procedure, a small volume (10 μl) of the stock solution is spread on the conductive surfaces of two glass plates coated with indium tin oxide (ITO). After removing all traces of the organic solvent using vacuum for at least one hour, the two glasses are assembled, with the conductive sides facing inwards, forming a chamber separated by a 2 mm thick Teflon frame. The chamber is gently filled with 100 mM sucrose solution and NaCl (0.01–10 mM) is added to adjust interior conductivity. The conductive sides of the ITO glass plates are connected to a function generator and an alternating current (3.6–8.0 Vpp, 10 Hz frequency) is applied for 1–2 h. Higher voltages within this range are used for higher M_w polymers. Vesicles with an average diameter of 50 μm and a large polydispersity are observed after about one hour. The vesicle solution is removed from the electroswelling chamber and diluted into an isotonic glucose and salt solution. The exterior fluid conductivity is adjusted by adding NaCl solution (0.01 mM to 10 mM concentrations). The lipids and low M_w polymersomes were grown at room temperature, while PS4 was heated to 60 °C.

3.2 Electrodeformation set-up

The electrodeformation experiments were conducted in a chamber (Eppendorf, Germany), which consists of a Teflon frame confined from above and below by two glass slides. A pair of parallel cylindrical electrodes with a radius of 92 μm and a separation of 0.5 mm are fixed to the lower glass. The chamber is connected to an AC function generator (Fluke PM5138A).

Table 1 Material properties of the amphiphiles used in this study. In all polymer systems, the 1,2-butadiene content is about 90%

Name	Amphiphile	M_n (kDa)	M_w/M_n	ϕ (%)
LS1	POPC	0.760	—	30
PS1	$n = 21$, $m = 14$	1.2-*b*-0.6	1.17	33
PS2	$n = 32$, $m = 20$	1.8-*b*-0.9	1.05	33
PS3	$n = 47$, $m = 34$	2.5-*b*-1.5	1.04	37.5
PS4	$n = 110$, $m = 89$	6.5-*b*-3.9	1.10	37.5

3.3 Optical microscopy and imaging

Due to the differences in density and refractive index between the sucrose and glucose solutions, the vesicles are stabilized by gravity close to the bottom of the chamber and have good contrast when observed with phase contrast microscopy. An inverted microscope Axiovert 135 (Zeiss, Germany) equipped with 20 × Ph2 objectives was used to image the vesicle under phase contrast mode. Images were recorded with a digital camera. A temperature control block was used to increase the temperature to 60 °C for the experiments with vesicles made of PS4 polymers since no appreciable deformation was detected at room temperature. At higher temperature, the fluid properties of the membrane are enhanced and the PS4 polymersomes deform more readily. The lower M_w polymer PS1–PS3 and lipid (POPC) membranes exhibited fluid behavior at room temperature, therefore all experiments with these systems were conducted at room temperature.

For routine observations, vesicle selection and electrodeformation measurements, the samples were illuminated with a halogen lamp. The vesicles were allowed sufficient time to relax to a steady state shape whenever experimental parameters (*i.e.* frequency or field strength) were changed. An image of the steady state shape is then taken and analyzed using in-house image analysis software. The image analysis software detects the phase contrast contour of the vesicle membrane with subpixel resolution[45] and fits the vesicle contour by a Fourier series[46] (alternatively, the shape can be fitted by an ellipse to a set of points). The second mode of the Fourier series expansion determines the two semi axes $a_{\parallel}$ and $a_{\perp}$, which are used to extract the degree of deformation D.

4 Results and discussion

Eqn (2) indicates that the oblate–prolate transition frequency f_c depends on membrane capacitance, vesicle size, and conductivities of the inner and outer solutions. Next we examine the variation of the transition frequency with these parameters and show how to extract data for the membrane capacitance using the dependence of f_c on vesicle size.

4.1 Effect of membrane thickness and vesicle radius

As seen from eqn (2), the transition frequency is inversely proportional to vesicle radius. By sampling the prolate–oblate transition for different sized vesicles (same membrane composition and conductivity conditions) in a single experiment, the effect of radius can be isolated. For that purpose we apply the electric field to a collection of vesicles. To avoid interactions between vesicles, the vesicle suspension is sufficiently dilute so that vesicles are isolated from each other.

Fig. 3 shows that the transition frequency increases linearly with the inverse vesicle radius. With all other parameters known (solution conductivities and vesicle equilibrium radius), the only unknown left is the membrane capacitance, which is used to fit the data. The values for the membrane capacitance obtained from the fits are in the range of 0.065–0.71 μF cm^{-2}, which are in agreement with data previously reported in the literature.[21,30]

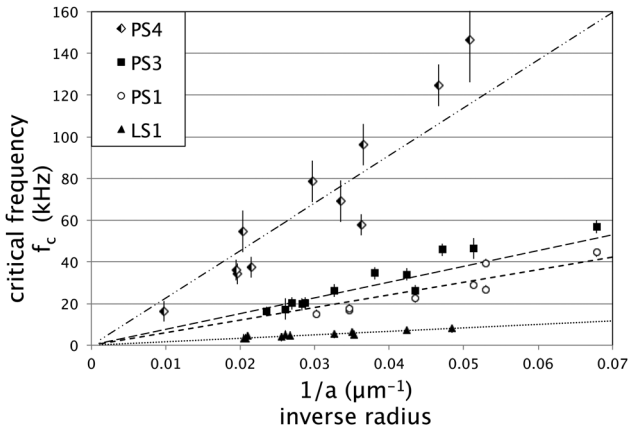

Fig. 3 Critical frequency, f_c, for the oblate–prolate transition as a function of inverse radius of vesicles made of POPC and polymersomes made of PS1, PS3 and PS4. The solution conductivities are $\lambda_{in} = 130$ μS cm^{-1} and $\lambda_{ex} = 520$ μS cm^{-1} ($\Lambda = 0.25$). The data is fit to theoretical transition values with $C_m = 0.71$ μF cm^{-2} for POPC, $C_m = 0.26$ μF cm^{-2} for PS1, $C_m = 0.16$ μF cm^{-2} for PS3, and $C_m = 0.065$ μF cm^{-2} for PS4. The relative errors of all experimental systems are comparable. The axis scale obscures the error in systems PS1 and LS1.

The membrane capacitance is inversely proportional to the bilayer thickness, which in turn exhibits a power-law dependence on the molecular weight $d \sim M_w^b$, where the exponent b lies within the theoretical bounds of 0.5 (random Gaussian coil) and 1 (full stretch).[38,47] Hence, the membrane capacitance should also follow a power law $C_m \sim M_w^{-b}$ provided the membrane permittivity ε_m is the same. Fig. 4 confirms this conclusion. The data show that C_m decreases with M_w complying with a power-law relationship with an exponent lying in the expected range, $0.5 < b < 1.0$. This is in agreement with the reported behavior of PBd-PEO membranes.[48,49] Note that for PS4, the capacitance is measured at higher temperature, which likely influences the membrane structure and may lead to a deviation from the suggested power law.

4.2 Effect of salt concentration (solution conductivity)

The charge near the membrane surfaces forms diffuse clouds. These ionic double layers have a capacitance C_D that acts in series with the bilayer capacitor[50] and increases the experimentally measured capacitance

$$\frac{1}{C_m} = \frac{1}{C_B} + \frac{1}{C_{D,in}} + \frac{1}{C_{D,ex}} \quad (4)$$

where C_B is the capacitance of the "bare" bilayer and the subscripts in and ex refer to inner and outer double layers at the vesicle membrane. Since the Debye time for diffusion across the double-layer thickness is of the order of nano-seconds, on the time scale of the applied kHz AC field the electric double layers are quasi-steady and equilibrium. Assuming a linear capacitor model (appropriate for the voltages in our experiments), the double-layer capacitance is equal to the capacitance of a planar capacitor with a thickness of one Debye length κ_D and the dielectric constant of the solution.[41,51–54]

Increasing the ionic strength of the solutions decreases the Debye length (for a 1 : 1 electrolyte $\kappa_D = 0.303c^{-1/2}$ nm, where c is the electrolyte concentration in M). Accordingly, the combined capacitance of the electrolyte–membrane system increases with ion concentration to an upper limit given by the bilayer capacitance C_B.

The effect of the diffuse layers is most significant when C_D and C_B are of comparable magnitude. This is true for low salt concentrations and/or large values of C_m. Hence, the measurements for POPC at low salt concentrations show more pronounced deviation between the effective (measured) and bilayer capacitance as seen in Fig. 5. The measurements of PS1–PS4 polymer membranes showed minimal variation due to their lower capacitance, which is documented in Fig. 6 and Table 2.

Bulk conductivities also influence the accuracy of the experimental data. Membrane charging depends on how fast charges are brought to the surface, which is quantified by the bulk conductivities. Hence, the transition frequency is sensitive to errors in determining the conductivities. Evaporation, vesicle

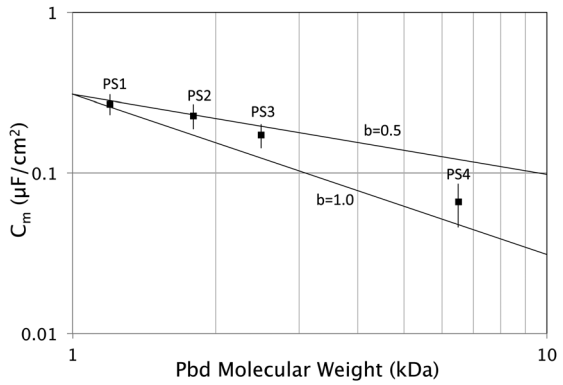

Fig. 4 Membrane capacitance as a function of polymer molecular weight. Error bars indicate the standard deviation of capacitance values determined from a set of measurements. The theoretical capacitance is based on a thickness to molecular weight relationship $d \sim M_w^{-b}$, where $0.5 < b < 1.0$ and the dielectric constant is assumed to be independent of molecular weight. The solid lines represent the power-law relationships for $b = 0.5$ and $b = 1.0$.

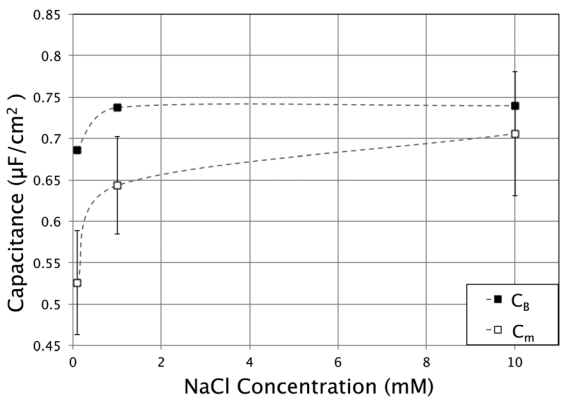

Fig. 5 Total specific membrane capacitance at different interior solution conductivities (salt concentrations) for POPC vesicles (LS1). The bilayer capacitance is obtained by subtracting the contribution of the double layers according to eqn (4). The exterior conductivity was varied to produce a conductivity ratio within $\Lambda = 0.1$–0.3. The lines are plotted to guide the eye. The error bars represent standard deviation.

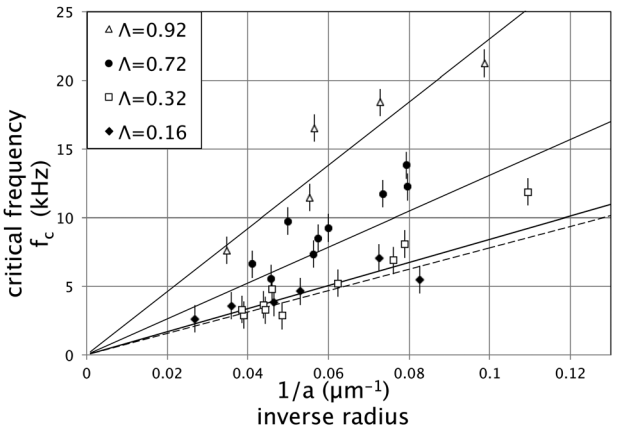

Fig. 6 Transition frequency for PS2 polymersomes with interior conductivity $\lambda_{in} = 18$ μS cm^{-1} in external solutions of different conductivity. All data are fit with $C_m = 0.22$ μF cm^{-2} using eqn (2).

Table 2 Capacitance values for PBd$_n$-*b*-PEO$_m$ measured with the electrodeformation method, C_m, and corrected for the effect of the Debye layers, C_B. The uncertainty is determined using error propagation and weighted sample variance for uncertainties associated with conductivity measurements and transition frequency

PBd$_n$-*b*-PEO$_m$	C_m (μF cm^{-2})	C_B (μF cm^{-2})	Error (SD)
PS1	0.256	0.270	±0.032
PS2	0.212	0.227	±0.039
PS3	0.166	0.172	±0.025
PS4	0.065	0.066	±0.014

rupture and impurities during preparation introduce variability in bulk conductivities, in particular, the conductivity of the small volume of solution in which the vesicles are grown. As a result, λ_{in} may change significantly. In order to determine the error in the interior conductivity, vesicles were diluted into a range of exterior solutions close to $\Lambda \sim 1$. The samples are then subjected to an AC electric field in the intermediate frequency range, 300 kHz, where the vesicle deformation should be oblate for $\Lambda < 1$ and prolate for $\Lambda > 1$. The $\Lambda = 1$ ($\lambda_{ex} = \lambda_{in}$) delineates the samples with prolate and oblate shapes. In this way, knowing λ_{ex}, the post preparation λ_{in} can be estimated. This method was used for each individual batch of vesicles. We found that the interior bulk conductivities could change by as much as 20–30% compared to the original solution in which they were grown. This explains the scatter in the data seen in Fig. 6.

4.3 Effect of field strength

The capacitance of BLMs (with solvent) increases quadratically with the applied voltage,[21,23,55,56] which has been attributed to membrane thinning associated with solvent exclusion. Enhanced fluctuations are also speculated to contribute to this effect.[57] For a spherical vesicle, the membrane electrostriction depends on the polar angle; it is maximal at the poles where the potential is largest. Therefore, the capacitance dependence on field strength is expected to be more complex.

Our measurements with lipid vesicles did not detect voltage dependence of the prolate–oblate transition frequency. We hypothesized that the polymer membranes could be more compressible due to the longer polymer chain length. However, Fig. 7 shows that although polymersome deformation increases with field strength, the frequency for the prolate–oblate transition does not change. This implies that the membrane thickness and capacitance are voltage-independent (in the investigated range of field strengths) in agreement with the reported behavior of solvent-free BLMs. An estimated 7% maximum areal strains shows that the polymersome is indeed not in the stretching regime,[43] and hence the membrane is not thinning due to stretching. Stronger fields are required in order to attain greater areal strain. However, in this case we discovered that polymersomes start to rotate. This behavior, illustrated in Fig. 8, is a novel, thus-far unreported feature of bilayer vesicles. In moderately strong fields ($E \sim 5$ kV m^{-1}), the oblately deformed polymersomes orient obliquely with respect to the field direction and the membrane rotates continuously. This dynamics is reminiscent of the rotation of fluid drops in a uniform electric field,[58] which is the analog of the Quincke rotation of rigid dielectric spheres or shells.[59,60] The tilted orientation makes the vesicle appear more prolate, which introduces a large error in determining the prolate–oblate transition. In stronger fields ($E >$ 10 kV m^{-1}) the effect is even more dramatic with the entire polymersome tumbling.

5 Conclusions

We demonstrate that the frequency-dependent vesicle deformation can serve as a facile method to determine the specific capacitance of bilayer membranes. The linear dependence of the transition frequency on inverse vesicle radius can be fitted using eqn (2) with the membrane capacitance as an adjustable parameter. Bilayers made of lipids have higher capacitance, $C_m = 0.71$ μF m^{-2} for POPC than block-copolymers, *e.g.*, $C_m = 0.26$ μF m^{-2} for PBd$_{21}$-*b*-PEO$_{14}$, which correlates with the polymer's

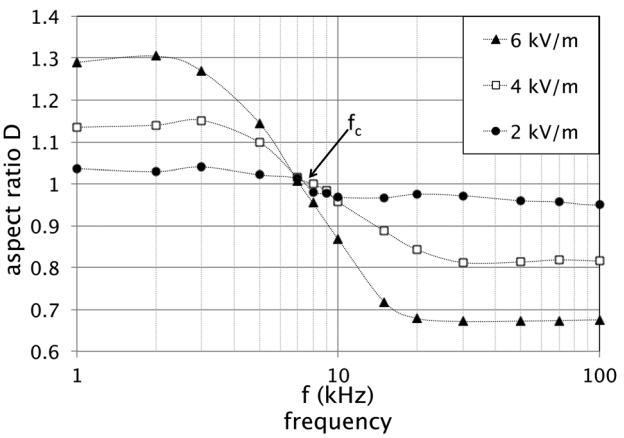

Fig. 7 Shape elongation D variation with frequency at different field strengths $E_0 = 6$, 4, 2 kV m^{-1} for a 18 μm polymersome (PS1) and conductivity conditions $\lambda_{in} = 20$ μS cm^{-1} and $\lambda_{ex} = 40$ μS cm^{-1}. The transition between prolate and oblate ellipsoids occurs between 7–8 kHz for all field strengths, where $D = 1$ corresponds to a spherical shape. There is no observable field strength dependence for the transition frequency (*i.e.* all transitions occur at the same approximate value). The greatest deformation observed, aspect ratio $D = 1.3$, corresponds to an areal strain $\Delta A/A = 7\%$.

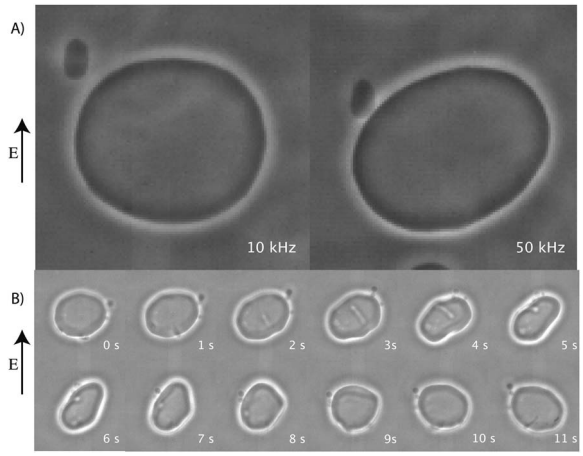

Fig. 8 (A) A polymersome (PS2) with 22 μm radius, solution conductivities $\lambda_{in} = 5$ μS cm^{-1} and $\lambda_{ex} = 25$ μS cm^{-1} ($\Lambda = 0.2$), in an electric field $E = 4$ kV m^{-1}. Upon increase of frequency (from 10 to 50 kHz) the vesicle evolves towards a steady tilted orientation with respect to the applied field. (B) A polymersome (PS2) with 24 μm radius, solution conductivities $\lambda_{in} = 5$ μS cm^{-1} and $\lambda_{ex} = 56$ μS cm^{-1} ($\Lambda = 0.09$), in an electric field $E = 40$ kV m^{-1}, frequency $f = 100$ kHz. The vesicle exhibits unsteady tumbling.

thicker membrane. The capacitance shows a power-law dependence on polymer molecular weight. The membrane capacitance was found to increase with bulk salt concentration due to the thinning of the ion double layer adjacent to the membrane surfaces. The electric field strength does not affect the capacitance, indicating that membranes do not experience significant thinning due to electrostriction. This method can be applied to vesicles prepared from lipid extracts of the plasma membrane of cells, *e.g.*, human red blood cells, to investigate the influence of naturally present transmembrane proteins. Knowledge about the electrical properties of model membranes with more complex composition as well as those of biological membranes is essential for correctly evaluating the mechanisms and conditions of electro-poration and -manipulation applied in technologies such as gene transfer and drug delivery.

Acknowledgements

PFS acknowledges partial financial support by NSF grants CBET-1117099 and OISE-1032280.

References

1 R. Pethig and D. Kell, *Phys. Med. Biol.*, 1987, **32**, 933–970.
2 K. Cole, *Membranes, ions and impulses*, University of California Press, 1968.
3 L. Gentet, G. Stuart and J. Clements, *Biophys. J.*, 2000, **79**, 314–320.
4 B. Bean, *Nat. Rev. Neurosci.*, 2007, **8**, 451–465.
5 E. Neumann, A. E. Sowers and C. A. Jordan, *Electroporation and electrofusion in cell biology*, Plenum Press, New York, 1989.
6 K. Schoenbach, S. Beebe and E. Buescher, *Bioelectromagnetics*, 2001, **22**, 440–448.
7 J. D. Deng, K. H. Schoenbach, E. S. Buescher, P. S. Hair, P. M. Fox and S. J. Beebe, *Biophys. J.*, 2003, **84**, 2709–2714.
8 J. T. Schwalbe, P. M. Vlahovska and M. J. Miksis, *Phys. Fluids*, 2011, **23**, 041701.
9 H. P. Schwan, *Electroporation and electrofusion in cell biology*, Plenum Press, 1989, pp. 3–21.
10 K. D. Gillis, *Single Channel Recording*, Plenum, New York, 1995, pp. 155–198.
11 T. B. Jones, *Electromechanics of particles*, Cambridge University Press, New York, 1995.
12 K. R. Foster and H. P. Schwan, *Crit. Rev. Biomed. Eng.*, 1989, **17**, 25–104.
13 H. G. L. Coster, T. C. Chilcott and A. C. F. Coster, *Bioelectrochem. Bioenerg.*, 1996, **40**, 79–98.
14 T. Sun and H. Morgan, *Microfluid. Nanofluid.*, 2010, **8**, 423–443.
15 F. Bordi, C. Cametti and S. Sennato, *Advances in planar lipid bilayers and liposomes vol. 4*, Elsevier, 2006, pp. 282–320.
16 E. Prodan, C. Prodan and J. H. Miller, *Biophys. J.*, 2008, **95**, 4174–4182.
17 H. T. Tien, *Bilayer Lipid Membranes (BLM): Theory and Practice*, Marcel Dekker, New York, 1974.
18 H. G. L. Coster, *Planar lipid bilayers (BLMs) and their applications, Chapter 2*, Elsevier, 2003, pp. 75–108.
19 Y. A. Chizmadzhev and V. F. Pastushenko, *Biologicheskie Membrany*, 1989, **6**, 1013–1045.
20 A. Babakov, L. N. Ermishkin and E. A. Liberman, *Nature*, 1966, **210**, 953–955.
21 R. Benz and K. Janko, *Biochim. Biophys. Acta, Biomembr.*, 1976, **455**, 721–738.
22 S. H. White, *Biophys. J.*, 1970, **10**, 1127–1148.
23 O. Alvarez and R. Latorre, *Biophys. J.*, 1978, **21**, 1–17.
24 M. Naumowicz and Z. A. Figaszewski, *J. Membr. Biol.*, 2011, **240**, 47–53.
25 P. Kramar, D. Miklavcic, M. Kotulska and A. M. Lebar, *Advances in Planar Lipid Bilayers and Liposomes, vol. 11*, Elsevier, 2010, pp. 29–66.
26 R. Dimova, S. Aranda, N. Bezlyepkina, V. Nikolov, K. A. Riske and R. Lipowsky, *J. Phys.: Condens. Matter*, 2006, **18**, S1151–S1176.
27 R. Dimova, K. A. Riske, S. Aranda, N. Bezlyepkina, R. L. Knorr and R. Lipowsky, *Soft Matter*, 2007, **3**, 817–827.
28 R. Dimova, N. Bezlyepkina, M. D. Jordo, R. L. Knorr, K. A. Riske, M. Staykova, P. M. Vlahovska, T. Yamamoto, P. Yang and R. Lipowsky, *Soft Matter*, 2009, **5**, 3201–3212.
29 D. Needham and R. M. Hochmuth, *Biophys. J.*, 1989, **55**, 1001–1009.
30 H. Aranda-Espinoza, D. Hammer and D. Discher, *Phys. Rev. Lett.*, 2001, **87**, 208301.
31 M. Kummrow and W. Helfrich, *Phys. Rev. A: At., Mol., Opt. Phys.*, 1991, **44**, 8356–8360.
32 M. D. Mitov, P. Meleard, M. Winterhalter, M. I. Angelova and P. Bothorel, *Phys. Rev. E: Stat. Phys., Plasmas, Fluids, Relat. Interdiscip. Top.*, 1993, **48**, 628–631.
33 S. Aranda, K. A. Riske, R. Lipowsky and R. Dimova, *Biophys. J.*, 2008, **95**, L19–L21.
34 K. Antonova, V. Vitkova and M. D. Mitov, *Europhys. Lett.*, 2010, **89**, 38004.
35 P. M. Vlahovska, R. S. Gracia, S. Aranda-Espinoza and R. Dimova, *Biophys. J.*, 2009, **96**, 4789–4803.
36 T. Yamamoto, S. Aranda-Espinoza, R. Dimova and R. Lipowsky, *Langmuir*, 2010, **26**, 12390–12407.
37 P. Peterlin, *J. Biol. Phys.*, 2010, **36**, 339–354.
38 D. E. Discher and F. Ahmed, *Annu. Rev. Biomed. Eng.*, 2006, **8**, 323–341.
39 D. A. Hammer and D. E. Discher, *Annu. Rev. Mater. Res.*, 2001, **31**, 387–404.
40 P. M. Vlahovska, *Advances in Planar Lipid Bilayers and Liposomes, vol. 12*, Elsevier, 2010, pp. 103–146.
41 C. Grosse and H. P. Schwan, *Biophys. J.*, 1992, **63**, 1632–1642.
42 M. I. Angelova and D. S. Dimitrov, *Faraday Discuss. Chem. Soc.*, 1986, **81**, 303–311.
43 R. Dimova, U. Seifert, B. Poligny, S. Forster and H.-G. Dobereiner, *Eur. Phys. J. D*, 2002, **7**, 241–250.
44 S. Förster and E. Krämer, *Macromolecules*, 1999, **32**, 2783–2785.
45 R. S. Gracia, N. Bezlyepkina, R. L. Knorr, R. L. Lipowsky and R. Dimova, *Soft Matter*, 2010, **6**, 1472–1482.
46 J. Pecreaux, H.-G. Dobereiner, J. Prost, J.-F. Joanny and P. Bassereau, *Eur. Phys. J. E*, 2004, **13**, 277–290.
47 C. LoPresti, H. Lomas, M. Massignani, T. Smart and G. Battaglia, *J. Mater. Chem.*, 2009, **19**, 3576–3590.
48 M. Matsen and F. Bates, *Macromolecules*, 1995, **28**, 8884–8886.
49 G. Battaglia and A. Ryan, *J. Am. Chem. Soc.*, 2005, **127**, 8757–8764.
50 D. Laver, *Advances in Planar Lipid Bilayers and Liposomes, vol. 9*, Elsevier, 2009, pp. 87–105.
51 D. A. Saville, *Annu. Rev. Fluid Mech.*, 1997, **29**, 27–64.

52 T. M. Squires and M. Z. Bazant, *J. Fluid Mech.*, 2004, **509**, 217–252.
53 M. Z. Bazant, K. Thornton and A. Ajdari, *Phys. Rev. E: Stat., Nonlinear, Soft Matter Phys.*, 2004, **70**, 021506.
54 F. Ziebert and D. Lacoste, *Advances in planar lipid bilayers and liposomes vol. 14*, Elsevier, 2011, pp. 64–95.
55 P. Schoch, D. Sargent and R. Schwyzer, *J. Membr. Biol.*, 1979, **46**, 7189.
56 S. H. White and W. Chang, *Biophys. J.*, 1981, **36**, 449–453.
57 S. L. Leikin, *Biologicheskie Membrany*, 1985, **2**, 820–831.
58 P. F. Salipante and P. M. Vlahovska, *Phys. Fluids*, 2010, **22**, 112110.
59 T. B. Jones, *IEEE Trans. Ind. Appl.*, 1984, **20**, 845–849.
60 I. Turcu and C. M. Lucaciu, *J. Phys. A: Math. Gen.*, 1989, **22**, 995–1003.

